Supporting information

Relationship between supramolecular assembly and charge-carrier mobility in perylenediimide derivatives: The impact of side chains

Falk May,[1,*] Valentina Marcon,[2,†] Michael Ryan Hansen,[1,‡] Ferdinand Grozema,[3,§] and Denis Andrienko[1,¶]

[1] *Max Planck Institute for Polymer Research, Ackermannweg 10, 55128 Mainz, Germany*
[2] *Center of Smart Interfaces, Petersenstr. 32, 64287 Darmstadt, Germany*
[3] *DelftChemTech, Delft University of Technology, Julianalaan 136, 2628 BL Delft, The Netherlands*

(Dated: April 14, 2011)

Supporting information

A. Force field

We used the GROMACS package to perform MD simulations in the NPT ensemble [1]. In the case of $C_{8,7}$–PDI the model potential is based on the OPLS all-atom force field except for the side chains where we used an OPLS united-atom representation. As there was no united-atom representation for the glycol side chain we used a full all-atom representation for TEG–PDI. Since OPLS does not have parameters of the bonded potentials linking side chains with the extended aromatic core, we parameterized these potentials assuming that they are identical for the glycol and alkyl side chain. First the improper dihedral describing the movement of the first carbon atom of the side chain out of the plane of the core was scanned by fixing the corresponding angle to values between 0° and 32° and optimizing the molecular geometry for each angle using DFT calculations and the B3LYP functional with the 6-31g(d) basis set. The potential energy of each structure was then evaluated using the known force field parameters with this improper dihedral switched off. The difference between the first principles and force-field-based energies was then fitted yielding the parametrization constants. The resulting harmonic potential for the improper dihedral is shown as a solid line against the DFT result in the left part of Fig. 1. The equilibrium position is at 0° (in the planar configuration) and the harmonic constant takes a value of 99.0 kJ/mol. Then the proper dihedral describing the rotation of the side chain around the bond between the nitrogen atom of the core and the first carbon atom in the side chain was scanned using the MP2 method and the same basis set. The torsion potential is shown in the right part of Fig. 1 and has a minimum at around 60°. It was fitted using a periodic function

$$V = V_0 \left(1 + \cos\left(n\theta - \theta_0\right)\right) \tag{1}$$

with $V_0 = 26.31\,\mathrm{kJ/mol}$, $n = 2$ and $\theta_0 = 60°$.

Solid-State NMR

The 1D and 2D solid-state ^{1}H and ^{13}C MAS NMR experiments were performed on Bruker DRX 700 and Bruker AVANCE-III 850 spectrometers operating at Larmor frequencies of 700.1 (16.4 T) and 850.2 MHz (20.0 T), respectively. The experiments have been recorded using magic-angle spinning (MAS) double-resonance 2.5 mm probes or a 1.3 mm probe commercially available from Bruker, Rheinstetten, Germany. These probes supports spinning frequencies of up to 30.0 and 60.0 kHz, respectively. In case of the 2.5 mm probes a 90° pulse length of 2.5 μs (ν_{rf} = 100.0 kHz) was used for both ^{1}H and ^{13}C, whereas the 1.3 mm probe employed a pulse length of 1.5 μs (ν_{rf} = 100.0 kHz) for ^{1}H. 2D ^{1}H-^{1}H Double-Quantum Single-Quantum (DQ-SQ) correlation experiments were recorded using the Back-to-Back (BaBa) recoupling sequences [2, 3] for both excitation and reconversion of DQ coherences followed by a z-filter, set to one rotor period, prior to a final 90° pulse for creating transverse observable magnetization. All 2D ^{1}H-^{1}H DQ-SQ experiments have employed a phase cycling scheme of 16 steps in order to select DQ coherences, a recycle delay of 2-s, and 16 scans per t_1 increment. The 2D ^{13}C{^{1}H} correlation spectra were recorded at 20.0 T using either Rotor-Encoded Polarization Transfer Heteronuclear Single Quantum Correlation (REPT-HSQC) [4] or Frequency-Switched Lee-Goldburg HETCOR (FSLG-HETCOR) pulse sequences [5, 6]. High-power heteronuclear decoupling was employed during acquisition using either TPPM or SPINAL-64 [7, 8]. In the case of ^{13}C{^{1}H} FSLG-HETCOR experiment, a recycle delay of 2-s, a total of 64 t_1 increments where each t_1 increment had a span of five basic FSLG blocks (81.6 μs), and a ramped CP step for transferring magnetization from ^{1}H to ^{13}C with a short duration of 500 μs to suppress weaker dipolar coupled spins. The LG scaling factor was determined experimentally on a powdered sample of adamantane to be 0.5. The ^{13}C{^{1}H}

*Electronic address: mayfalk@mpip-mainz.mpg.de
†Electronic address: marcon@csi.tu-darmstadt.de
‡Electronic address: hansen@mpip-mainz.mpg.de
§Electronic address: f.c.grozema@tudelft.nl
¶Electronic address: denis.andrienko@mpip-mainz.mpg.de

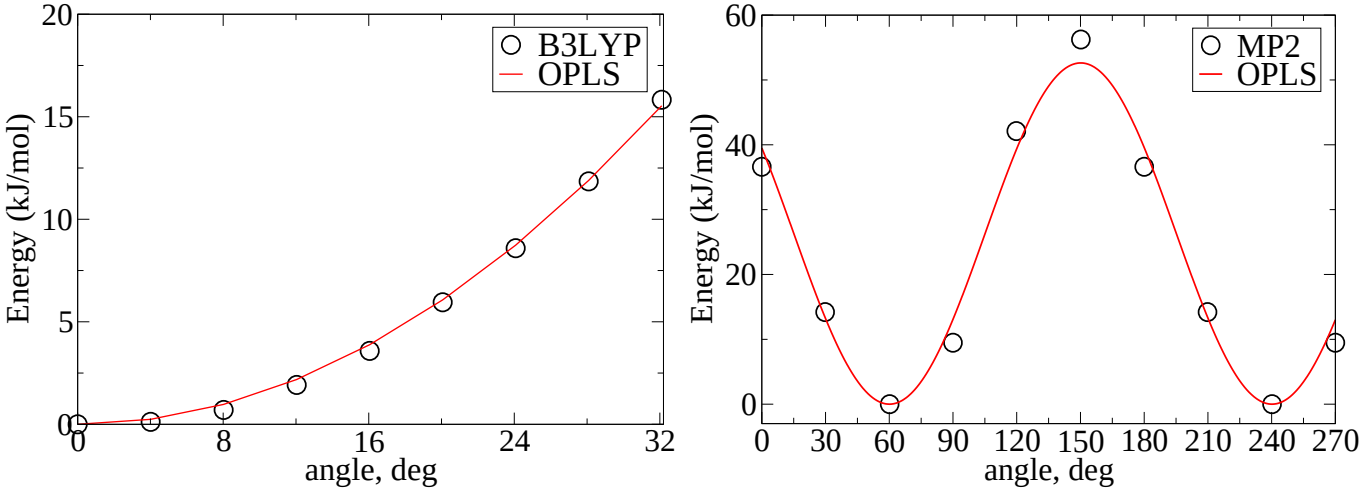

FIG. 1: Scans of the potential energy surface using first principles methods (symbols) and corresponding fits with empirical potentials (solid lines) for the improper (left) and dihedral (right) angles connecting the side chains to the aromatic core.

REPT-HSQC experiments used a recycle delay of 2-s, 64 t_1 increments, and symmetrical Rotational-Echo Double Resonance (REDOR) pulse trains (N_{exc}=N_{rec}) with N = 2 for recoupling an reconversion [4, 9]. In all cases phase-sensitive 2D spectra were recorded using States-TPPI [10]. The VT 1H MAS NMR experiments of TEG–PDI were performed on the DRX 700 spectrometer. Chemical shifts are reported relative to TMS using solid adamanate as an external reference [11] and the magic angle was adjusted before each measurement on solid KBr [12].

Pulse-radiolysis time-resolved microwave conductivity (PR-TRMC)

In order to perform PR-TRMC measurements, 30 mg and 40 mg powder samples of $C_{8,7}$–PDI and TEG–PDI, respectively were pressed into Perspex sample holders which were then introduced into a Ka-band (28-38 GHz) microwave cell. A uniform, micromolar concentration of charge carriers is generated into the sample by a 10 nanosecond pulse of 3 MeV electrons from a Van de Graaff accelerator. The decrease in the microwave power reflected by the sample cell indicates the changes in conductivity of the sample due to the formation of mobile charge carriers. The one-dimensional intracolumnar charge carrier mobility is determined using the following relationship

$$\mu = 3\frac{\Delta\sigma_{eop}}{D}\frac{E_p}{W_p}, \qquad (2)$$

where E_p is the average energy deposited per ionization event and W_p is the probability that initially formed ion-pairs survive until the end of the pulse. The value of E_p was 25 eV and the values of W_p, obtained as described in Ref. 14, were 0.513 for the $C_{8,7}$–PDI and 0.420 for TEG–PDI. The random orientation of the ordered columnar domains is taken into account by the prefactor 3.

Measured mobility μ is the sum of hole and electron mobilities, $\mu = \mu_+ + \mu_-$, since the PR-TRMC technique does not allow to distinguish the contribution of positive and negative charge carriers.

The temperature dependence of the charge carrier mobility is shown in Fig. 2. The absolute values of the mobility are around 0.15 $cm^2V^{-1}s^{-1}$ and 0.09 $cm^2V^{-1}s^{-1}$ at room temperature for the $C_{8,7}$–PDI and TEG–PDI, respectively. By increasing the temperature to 400K the mobility slightly decreases to 0.13 $cm^2V^{-1}s^{-1}$ and 0.07$cm^2V^{-1}s^{-1}$ respectively, without showing any abrupt changes which could be related to a phase transition.

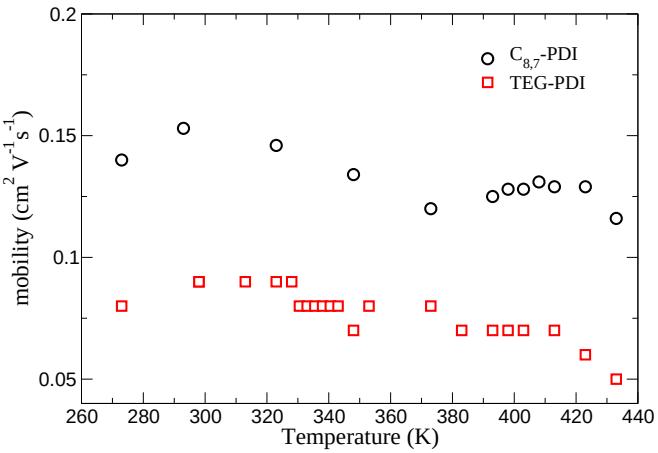

FIG. 2: Charge mobilities as a function of temperature as measured by the PR-TRMC technique.

Charge Transport Simulations

We compute charge carrier mobilities μ along all columns by solving a linearized master equation for one-dimensional transport

$$\frac{\partial P_i}{\partial t} = \sum_j (\omega_{ij} P_j - \omega_{ji} P_i)\,, \tag{3}$$

where P_i is the probability that the charge is on the molecule i in the column, ω_{ij} is the rate of charge transfer from the molecule i to the molecule j.

The charge velocity v along the applied electric field E (parallel to the columns, along the z-axis) is then calculated as

$$v = \sum_{ij} \omega_{ji} P_j z_{ji}, \tag{4}$$

and the mobility reads

$$\mu = \frac{v}{E}\,. \tag{5}$$

The hopping rates ω_{ij} are obtained from the high temperature limit of non-adiabatic Marcus theory

$$\omega_{ij} = \frac{J_{ij}^2}{\hbar}\sqrt{\frac{\pi}{\lambda k_{\mathrm{B}} T}}\exp\left[-\frac{(\Delta G_{ij} - \lambda)^2}{4\lambda k_{\mathrm{B}} T}\right]. \tag{6}$$

Here, J_{ij} is the electronic transfer integral between neighboring molecules, λ is the reorganization energy, $\Delta G_{ij} = E z_{ij}$ is the change in charge energy due to the applied electric field in the z-direction, and z_{ij} is the projected on the field distance between centers of mass of molecules.

For computation of transfer integrals, diabatic states were constructed by replacing the slightly deformed PDI-cores from MD snapshots by geometry optimized rigid copies, while retaining their orientations. Geometry optimization for the PDI-core was performed using the B3LYP hybrid functional and 6-311G(p,d) basis set, as implemented in the GAUSSIAN package [15].

The transfer integrals for the nearest neighbors were computed using a highly optimized ad hoc code which has been shown to give very similar results to density functional theory at a fraction of computational cost [16]. HOMO and LUMO orbitals of a neutral molecule were used to calculate transfer integrals for holes and electrons, respectively (frozen orbital approximation). The resulting transfer integral distributions for holes and electrons are displayed in Fig. 3.

The reorganization energy for holes was calculated as [17]

$$\lambda_+ = E^{(A1)}(A^+) - E^{(A1)}(A) + E^{(D2)}(D) - E^{(D2)}(D+)\,. \tag{7}$$

Here $E^{(A1)}(A^+)$ is the energy of neutral molecular acceptor $A1$ at the cation geometry A^+, while $E^{(A1)}(A)$ denotes its energy at the neutral geometry, and similar for the molecular donor $D2$. Similar expression was used for electrons.

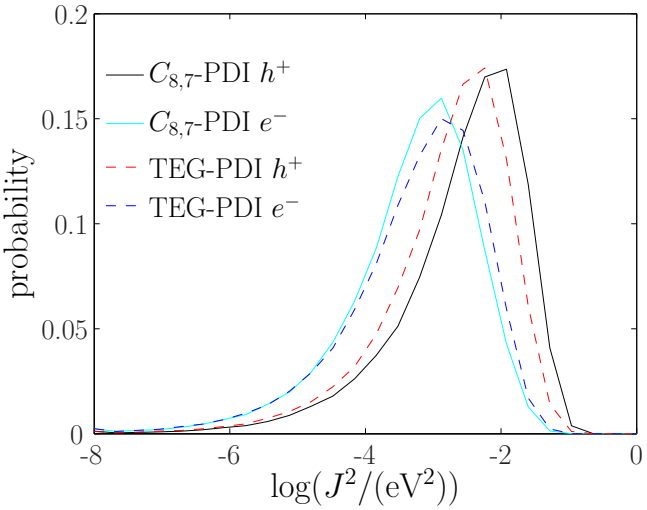

FIG. 3: Distribution of transfer integrals for holes and electrons in the two PDI derivatives. Orbital overlap favors hole transport in $C_{8,7}$–PDI and makes electron transport in both derivatives less efficient.

The values of $\lambda_+ = 0.14$eV and $\lambda_- = 0.24$eV indicate higher mobilities for holes, since higher λ means lower mobility if $|z_{ij}eE| < \lambda$, which is the case for electric fields used here, $E_z = 10^5 - 10^7$V/m.

One can separate the effect of the reorganization energy from that of transfer integrals on the charge mobility. Assuming a linear dependence of mobility on the rate, $\mu \propto \omega$, and expanding Marcus rates for both holes and electrons, we obtain

$$\frac{\mu_+}{\mu_-} = \frac{J_+^2}{J_-^2}\sqrt{\frac{\lambda_-}{\lambda_+}}\exp\left(\frac{\lambda_+ - \lambda_-}{4k_{\mathrm{B}}T}\right) = \frac{J_+^2}{J_-^2}F_\lambda \tag{8}$$

In our case $F_\lambda \approx 4$, i. e. hole transport is four times faster than electron transport in both derivatives due to the difference in the reorganization energies. The shift in the transfer integral distributions, which can be seen from Fig. 3, leads to a similar speed up for both derivatives, again in favor of holes.

References

[1] Lindahl, E.; Hess, B.; van der Spoel, D. *J. Mol. Mod.*, **2001**, *7*, 306–317.
[2] Feike, M.; Demco, D. E.; Graf, R.; Gottwald, J.; Hafner, S.; Spiess, H. W. *J. Magn. Res. Ser. A*, **1996**, *122*, 214–221.
[3] Feike, M.; Graf, R.; Schnell, I.; Jager, C.; Spiess, H. W. *J. Am. Chem. Soc.*, **1996**, *118*, 9631–9634.
[4] Saalwächter, K.; Schnell, I. *Solid State Nucl. Magn. Reson.*, **2002**, *22*, 154–187.
[5] Bielecki, A.; Kolbert, A.; Levitt, M. *Chem. Phys. Lett.*, **1989**, *155*, 341–346.

[6] van Rossum, B.; Forster, H.; deGroot, H. *J. Magn. Reson.*, **1997**, *124*, 516–519.
[7] Bennett, A.; Rienstra, C.; Auger, M.; Lakshmi, K.; Griffin, R. *J. Chem. Phys.*, **1995**, *103*, 6951–6958.
[8] Fung, B.; Khitrin, A.; Ermolaev, K. *J. Magn. Reson.*, **2000**, *142*, 97–101.
[9] Gullion, T.; Schaefer, J. *J. Magn. Reson.*, **1989**, *81*, 196–200.
[10] Marion, D.; Ikura, M.; Tschudin, R.; Bax, A. *J. Magn. Res.*, **1989**, *85*, 393–399.
[11] Morcombe, C. R.; Zilm, K. W. *J. Magn. Res.*, **2003**, *162*, 479–486.
[12] Frye, J. S.; Maciel, G. E. *J. Magn. Res.*, **1982**, *48*, 125–131.
[13] Hansen, M. R.; Graf, R.; Sekharan, S.; Sebastiani, D. *J. Am. Chem. Soc.*, **2009**, *131*(14), 5251–5256.
[14] van de Craats, A. Thesis delft university of technology, delft. Master's thesis, Delft University of Technology, 2000.
[15] Frisch, M. J.; *et al.* Gaussian 03, Revision C. 02. Gaussian, Inc. , Wallingford, CT, 2004.
[16] Kirkpatrick, J. *Int. J. Quant. Chem.*, **2007**, *108*, 51–56.
[17] Lemaur, V.; Da Silva Filho, D.; Coropceanu, V.; Lehmann, M.; Geerts, Y.; Piris, J.; Debije, M.; Van de Craats, A.; Senthilkumar, K.; Siebbeles, L.; Warman, J.; Bredas, J.; Cornil, J. *J. Am. Chem. Soc.*, **2004**, *126*, 3271– 3279.